Variation in the urban vegetation, surface temperature, air temperature nexus

Sheri A. Shiflett [a], Liyin L. Liang [a,e], Steven M. Crum [a], Gudina L. Feyisa [b], Jun Wang [c,d], G. Darrel Jenerette [a,*]

[a] Department of Botany and Plant Sciences, University of California, Riverside, California, USA
[b] Department of Natural Resource Management, Jimma University, Ethiopia
[c] Center for Global and Regional Environmental Research, University of Iowa, Iowa City, Iowa, USA
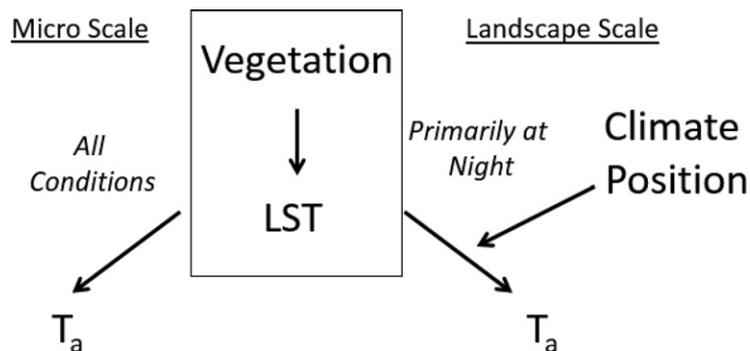[d] Department of Chemical and Biochemical Engineering, University of Iowa, Iowa City, Iowa, USA
[e] School of Science, University of Waikato, Hamilton, New Zealand

HIGHLIGHTS

- We investigated the vegetation – air temperature – land surface temperature nexus in southern California.
- We coupled 300 in-situ air temperature sensors with airborne measurements of a vegetation index and surface temperature.
- Vegetation was associated with cooler land surface temperature during the day and air temperature at night.
- Vegetation provides cooling benefits although the effects on microclimate vary by temperature, vegetation, and time of day.

GRAPHICAL ABSTRACT

ABSTRACT

Our study examines the urban vegetation – air temperature (T_a) – land surface temperature (LST) nexus at micro- and regional-scales to better understand urban climate dynamics and the uncertainty in using satellite-based LST for characterizing T_a. While vegetated cooling has been repeatedly linked to reductions in urban LST, the effects of vegetation on T_a, the quantity often used to characterize urban heat islands and global warming, and on the interactions between LST and T_a are less well characterized. To address this need we quantified summer temporal and spatial variation in T_a through a network of 300 air temperature sensors in three sub-regions of greater Los Angeles, CA, which spans a coastal to desert climate gradient. Additional sensors were placed within the inland sub-region at two heights (0.1 m and 2 m) within three groundcover types: bare soil, irrigated grass, and underneath citrus canopy. For the entire study region, we acquired new imagery data, which allowed calculation of the normalized difference vegetation index (NDVI) and LST. At the microscale, daytime T_a measured along a vertical gradient, ranged from 6 to 3 °C cooler at 0.1 and 2 m, underneath tall canopy compared to bare ground respectively. At the regional scale NDVI and LST were negatively correlated ($p < 0.001$). Relationships between diel variation in T_a and daytime LST at the regional scale were progressively weaker moving away from the coast and were generally limited to evening and nighttime hours. Relationships between NDVI and T_a were stronger during nighttime hours, yet effectiveness of mid-day vegetated cooling increased substantially at the most arid region. The effectiveness of vegetated T_a cooling increased during heat waves throughout the region. Our

* Corresponding author at: Department of Botany and Plant Sciences, University of California, Riverside, California 92512, USA.
   E-mail address: darrel.jenerette@ucr.edu (G.D. Jenerette).

findings suggest an important but complex role of vegetation on LST and T_a and that vegetation may provide a negative feedback to urban climate warming.

1. Introduction

Urbanization is characterized by extensive land use transformation and altered surface thermal characteristics (Kalnay and Cai, 2003). Increased heat capacity associated with built environments leads to warmer nighttime urban air temperatures (T_a), commonly described as the urban heat island (Oke, 1973; Santamouris, 2015). During the day, limited evaporation and low albedos of built surfaces are associated with greater daytime urban radiant temperatures observed from remote sensors, commonly referred as land surface temperature (LST; Jenerette et al., 2007). Notably, urbanization is associated with a high degree of spatial heterogeneity in thermal characteristics and as a result, there are large differences in intra-urban land surface and air temperatures (Upmanis et al., 1998; Svensson and Eliasson, 2002; Huang et al., 2011; Hall et al. 2016; Jenerette et al., 2016) that change substantially at daily and seasonal scales (Jenerette et al., 2013; Coseo and Larsen, 2014). Both components of urban temperature variation have important implications for the well-being of urban residents. T_a has been repeatedly found to influence energy demand through its relation to air conditioning habits and human health through heat-related illness (Kalkstein, 1991; Santamouris et al., 2001; Hondula and Barnett, 2014). LST is also an important variable in the study of urban climates (Voogt and Oke, 2003) and has been shown to directly correlate with heat-related health incidents (Laaidi et al., 2012; Vanos, 2015; Jenerette et al., 2016). Uncertainties in understanding spatial and temporal variation in both T_a and LST in urban environments undermine a robust understanding of the drivers of urban microclimates and relationships between LST and more widely characterized T_a. Resolving the uncertainties at the vegetation-LST-T_a nexus is essential for designing urban landscapes that minimize the many negative consequences of high urban temperatures.

LST modulates T_a of the lower layer of the urban atmosphere and is a primary factor in determining surface radiation and energy exchange, the internal climate of buildings, and human comfort in cities (Voogt and Oke, 2003). Intra-urban T_a differences of >8 °C have been reported (Upmanis et al., 1998; Svensson and Eliasson, 2002; Stabler et al., 2005). LST variation within a city can be larger, spanning >20 °C (Jenerette et al., 2007). Reconciling causes and correlations in variation between these two urban temperature components remains a persistent challenge (Hartz et al., 2006). The few studies of the relationships between LST and T_a have had mixed results with some studies showing strong correlations and others not identifying relationships (Hartz et al., 2006; Cheng et al., 2008; Schwarz et al., 2012). When T_a - LST linkages are observed they show diel variation; with some evidence of correlations at night but less so during the day (Kawashima et al., 2000). The diel variation may be in response to the effects of increased atmospheric mixing during the day compared to night and also thermal properties of different surfaces. While distinct indicators of urban microclimates, both daytime increases in LST and nighttime increases in T_a represent risks to human health in urban environments (Kalkstein, 1991; Harlan et al., 2014).

Increasing urban vegetation is becoming a widely used tool for reducing both urban T_a and LST (Kurn et al., 1994; Weng and Yang, 2004; McPherson et al., 2011; Gillner et al., 2015; Larsen, 2015). Urban vegetation has a particularly important role in cooling surface temperatures during the day via evapotranspiration, physical shading, and also by increased albedo and reflected radiation relative to paved surfaces (Imhoff et al., 2010; Jenerette et al., 2016). For instance, the albedo of green roofs, which ranges from 0.7 to 0.85, is much higher than the 0.1 to 0.2 albedo range of typical roofing surfaces such as bitumen, tar,

and gravel, and enables green roofs to reflect 20–30% of solar radiation (Berardi, 2014). Georgescu et al. (2014) suggested in a modeling study that urban adaptation strategies such as green roofing (i.e., highly transpiring), or cool roofing (i.e., highly reflective) can offset urban-induced air temperature warming in cities across the United States and also offset a significant percentage of future greenhouse gas-induced warming over large scales. Similarly, many empirical studies have shown that increasing vegetation and specifically, canopy cover can substantially reduce LST (Declet-Barreto et al., 2016).

The magnitude of vegetated LST cooling depends on multiple factors including local meteorological conditions and extent of vegetation cover. Different forms of vegetation, for example grass versus trees, may have different influences on local microclimate. Tree-shading of built surfaces can provide comparable surface cooling as transpiring grass and additional cooling benefits relative to grass (Armson et al., 2012; Vanos et al., 2016). For instance, Armson et al. (2012) showed tree shade reduced surface temperatures by up to 19 °C, compared to a 24 °C reduction in maximum surface temperature related to grass cover. Yet, grass cover had little effect on globe temperature, a metric incorporating the effects of radiation, T_a, and wind on human comfort, while shading reduced globe temperature by 5–7 °C. Diel and seasonal variation in correlations between vegetation and LST suggest much stronger coupling during midday and in warmer seasons, than at night and in cooler seasons (Buyantuyev and Wu, 2010; Jenerette and Potere, 2011; Myint et al., 2013; Jenerette et al., 2016). Similarly, spatial variation across a climate gradient of the correlation between vegetation and LST also suggest more effective cooling in hot, arid locations compared to milder, coastal locations (Tayyebi and Jenerette, 2016).

In contrast, the role of vegetation in reducing T_a is less well understood and linkages between vegetation cover and T_a are more variable than vegetation – LST relationships. Sampling campaigns directed toward evaluating the effects of individual trees, green spaces, green roofs, or the urban tree canopy have shown localized air cooling associated with vegetation (Hart and Sailor, 2009; Feyisa et al., 2014; Petralli et al., 2014; Santamouris, 2014; Yan et al., 2014; Coseo and Larsen, 2014; Gillner et al., 2015; Wang et al., 2015). However, other studies have found no detectable effects of vegetation on T_a (Grundström and Pleijel, 2014; Klemm et al., 2015) or only limited effects when comparing the endpoints between bare to vegetated land covers (Skelhorn et al., 2014). Where vegetation effects on urban T_a have been found, they vary in diel magnitudes and in response to differing weather conditions (Coseo and Larsen, 2014; Wang et al., 2015). Further, climate context may have large influences on connections between land surface and local T_a patterns (Hall et al., 2016).

To address the uncertainties in the vegetation-LST-T_a nexus, we investigated their relationships at micro- and regional-scales across the Greater Los Angeles region spanning a coastal to desert gradient. First, we asked how different dominant vegetation functional types affected microscale T_a patterns at an intermediate climate location. At microscales, we hypothesized that vegetation would decrease near-surface temperatures, with increased cooling associated with taller canopies. We further predicted the land cover effect would be greater at near surface than at 2 m above ground because of increased air mixing at higher locations. Second, we asked how the relationships between urban vegetation, LST, and T_a vary across a regional-scale coastal to desert climate gradient. We hypothesized that increased vegetation cover will reduce T_a and LST-T_a differences, regardless of micro- or regional-scale, due to increased surface shading and evapotranspiration associated with increasing vegetation cover. We predicted that microclimate and vegetation relationships would increase in magnitude with increasing distance

from the coast due to higher rates of evapotranspiration driven by higher vapor pressure deficits at arid sites. We also hypothesized that relationships between LST and T_a will become weaker across a climate gradient because warm air absorbs less heat from land surfaces than cool air due to a reduced thermal gradient. Finally, we asked how do the climate – vegetation interactions differ during an extreme heat wave event relative to a cool period? We hypothesized the cooling effect will be stronger during the heat wave because evapotranspiration will increase during warmer periods. This heat wave was selected for further analysis because it was a noted social event and the effects spanned across all three regions.

2. Methods

2.1. Study site

The Greater Los Angeles metropolitan area, the second largest urban region in the United States, comprises 5 counties (Los Angeles, Orange, Riverside, San Bernardino, and Ventura), several major cities, and 88,000 km². While the entire region is characterized by a Mediterranean climate of alternating cool-wet winters and hot-dry summers, urbanization also extends across a pronounced coastal to desert climate gradient with mean annual temperatures increasing from 17.7 °C, 18.6 °C, to 24.3 °C and mean annual precipitation decreasing from 474.2 mm, 262.2 mm to 140.2 mm, from coastal Los Angeles proper to increasingly arid Riverside and Palm Springs, CA respectively. Elevation of sampled regions was 74 ± 16 m in Los Angeles, 306 ± 43 m in Riverside, and 117 ± 23 m in Palm Springs. Land cover distributions are a complex mosaic (Jenerette et al., 2013) and urban vegetation including >200 tree species is extensive throughout the region (Clarke et al., 2013). Improved understanding of interacting relationships between climate, land cover, and surface energy balance parameters such as temperature and evaporation across the Greater Los Angeles megapolitan region are needed as the area includes >18 million inhabitants and increasing frequency of high temperature periods (Xu et al., 2012). Further, with a large climate gradient, which extends from the coast (23 °C mean maximum summer T_a) to desert (48 °C mean maximum summer T_a), the Los Angeles, CA metropolitan region is a particularly useful study area to investigate relationships between urban LST, T_a, and vegetation.

2.2. Microscale

A portion of this research was conducted at an agricultural research station located at the University of California Riverside, in Riverside, CA. In order to test the diel effect of vegetation cover on air temperature, Thermochron iButton sensors in custom-made white vented enclosures (similar to Hall et al., 2016) were placed at two heights (0.1 m and 2 m) above bare soil, irrigated grass, and underneath citrus canopy of two canopy heights (2 m and 4 m). Citrus canopy at 2 m height consisted of individual trees, which were spaced ~1.5 m apart, whereas, canopy at 4 m height consisted of rows of mature trees that formed closed canopies. Three replicates were sampled within each cover and height class.

2.3. Regional scale

We quantified temporal (i.e., diel and monthly) and spatial variation in T_a by placing a network of 300 Thermochron iButton sensors on urban trees in cities spanning the Los Angeles metropolitan region (Los Angeles, Riverside, and Palm Springs, CA) from June to September 2014 (Fig. 1). Sensor locations were identified through a spatially stratified design and then choosing the closest available tree to each designated sampling location. Each sensor was placed in a custom-made vented white plastic shield and attached to the tree in an inconspicuous location at approximately 2 m height. Trees provide practical sensor siting. Not only are trees accessible throughout the urban environment, but they enable consistent sampling height in unobtrusive locations,

discouraging sensor vandalism and theft (Doick et al., 2014). Wind speed data were obtained from California Irrigation Management Information System (CIMIS) using stations at the Integrated Regional Water Management Southern Region Office in Santa Monica, CA, the University of California Riverside's Agricultural Experiment Station, and at the Shadow Hills Golf Club in Indio, California (http://www.cimis.water.ca.gov/WSNReportCriteria.aspx).

2.4. Remote sensing

Our study uses AVIRIS Airborne Visible-Infrared Imaging Spectrometer (AVIRIS) and MODIS/ASTER Airborne Simulator (MASTER) data collected from the June 2014 Hyperspectral InfraRed Imager (HyspIRI) preparatory mission. The HyspIRI satellite mission, recommended by the 2007 National Research Council "Decadal Survey", will determine spectral and thermal characteristics of the world's ecosystems, enable monitoring of vegetation health, and detect and promote understanding of changes in terrestrial surface phenomena (Lee et al., 2015). HyspIRI is comprised of two instruments: a visible and shortwave infrared (VSWIR) imaging spectrometer and a thermal infrared (TIR) multispectral imager, together with a payload module enabling onboard processing and rapid transfer of selected data (Lee et al., 2015). The satellite will operate in low Earth orbit and provide global coverage every 5–6 days at 30–60 m spatial resolution. Prior to launch of the satellite, NASA initiated a HyspIRI preparatory campaign that uses similar technology as the proposed satellite, in the form of the AVIRIS and MASTER imagers, and was conducted throughout California (Roberts et al., 2012). For the HyspIRI preparatory mission, the imagers were mounted on the NASA ER-2 high-altitude aircraft, which collected VSWIR and TIR imagery simultaneously at approximately 20 km above sea level (Roberts et al., 2015).

Data products derived from this mission used here consisted of LST and NDVI, a widely used remotely sensed vegetation index (Tucker, 1979) and were of high quality. While a small portion of null values occurred within the NDVI layer, these locations were restricted to mountainous areas or along flight line edges. Anomalous or missing data values were not detected within our study sites. We used remotely-sensed data products to characterize targeted interacting relationships between climate, land cover, and surface energy balance parameters across the Greater Los Angeles, CA metropolitan area. Consistent with the large majority of urban LST studies, our remote sensing data were obtained from a single daytime flight. Overlapping flight lines captured all sites at approximately the same time of day (TOD) at 1300 h on June 13, 2014.

2.5. Land surface temperature

The MASTER sensor acquired data across the visible through mid-infrared wavelengths in 50 spectral bands and was used to derive LST at 50 m spatial resolution (Hook et al., 2001). Brightness data, including information on both surface temperature and surface emissivity, were collected by the MASTER sensor. Data were obtained from (http://masterprojects.jpl.nasa.gov/L2_Products), which was initially post-processed to level 2B, and included atmospheric correction, georectification, and georeferencing to the Universal Transverse Mercator projection system (datum WGS84, UTM Zone 11N). Subsequent post-processing of the MASTER data to include calculation of LST was conducted using ENVI/IDL. LST was extracted at each iButton location using ArcMap (ver 10.1, ESRI).

2.6. Normalized difference vegetation index

Vegetation indices are commonly developed from remotely sensed data to study changes in vegetative cover and LST associated with increasing urbanization (Roberts et al., 2015). For our study, NDVI was derived from AVIRIS data. AVIRIS delivers calibrated images of spectral
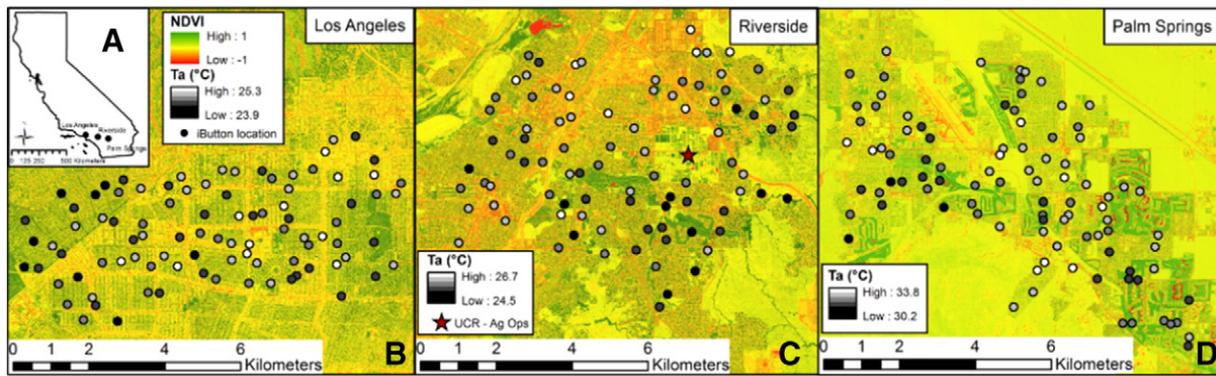
Fig. 1. Site description. Inset left panel (A): Coastal to desert transect of highly urbanized cities Los Angeles, Riverside, and Palm Springs, CA. (B, C, D) NDVI of each city overlain with Thermochron iButton sensor locations. Average T_a, calculated across all samples, for each sensor is represented by grayscale where darker colors indicate cooler temperatures. N.B. Microclimate iButton sensors were located within the University of California, Riverside (UCR) agricultural research station fields displayed on the Riverside, CA subregion map (vicinity represented by a star).

radiance in 224 spectral bands in 10 nm contiguous bands with wavelengths from 400 to 2500 nm (Hook et al., 2001). AVIRIS uses a scanning mirror to sweep back and forth, producing 677 pixels for the 224 detectors on each scan. Spatial resolution of AVIRIS for the HyspIRI preparatory campaign on June 13, 2014 was 20 m.

We obtained level 2B post processed data (http://aviris.jpl.nasa.gov/data), which included atmospheric correction, georectification, and georeferencing to the Universal Transverse Mercator projection system (datum WGS84, UTM Zone 11N). Atmospheric correction was conducted using the Atmospheric CORection Now software, which generates reflectance, column water vapor, and liquid water and is the standard for AVIRIS data (Roberts et al., 2015). We further processed AVIRIS data to obtain NDVI (Huete et al., 2002) using Eq. (1) (where B29 and B51 correspond to AVIRIS spectral channels 29 and 51 with wavelengths 0.64 μm and 0.83 μm). NDVI was averaged across a 50 m buffer at each iButton location and extracted using ArcMap (ver 10.1, ESRI). A 50 m buffer size was chosen to better align NDVI with a pixel size corresponding to LST and integrate mixed land cover surfaces within close proximity to each iButton location.

$$NDVI = (B29 - B51)/(B29 + B51) \qquad\qquad 1$$

2.7. iButton data QA/QC

iButtons were programmed using Thermodata Viewer software (ver 3.1.28, Thermodata) to record data hourly. iButton temperature readings were compared and calibrated by placement in climate controlled chambers at −12 °C, 4 °C, and at room temperature for a minimum of four hours in each environment pre- and post-deployment. No sensors were determined to yield erroneous temperature readings and all sensors recorded data to an accuracy of ±1.0 °C, regardless of temperature environment or deployment phase. Higher variation in iButtons was observed in cooler settings and was attributed to proximity to the front or sides of the climate-controlled containers. Temperature drift pre- and post-deployment was not observed; however, previous studies have suggested that iButtons should be calibrated at least every half year (Johnson et al., 2005).

Outliers of raw iButton data, considered as more than two and a half times interquartile ranges below the first quartile or above the third quartile, were removed prior to data analysis. <5% of the original data within each region was removed during the QA/QC process.

2.8. Data analysis

At the microscale, sensor averages were obtained for each land cover type at 0.1 m and 2 m heights. Data were extracted at multiple times of

day (0000, 0600, 1200, and 1800 h) and compared at each time period for each height class using one-way analysis of variance (ANOVA). At the regional scale, linear regression analysis was used to compare LST obtained at 1300 h (when flight lines covered all sites at approximately the same TOD) to NDVI, and T_a obtained from all iButtons within a region at this sampling time. Linear regression analysis was also used to compare diel and seasonal variation in T_a.

iButton data were subset to examine a late-season heat wave (DOY = 257–259) and post-heat wave interval (DOY = 262–264). At the microscale, lapse rates were calculated for each land cover type and at both height classes as the change in temperature over the change in height. Two-way ANOVA was used to determine interactions between land cover type and DOY class (i.e., heat wave, all data, and post-heat wave). At the regional scale, linear regression analysis was used to compare NDVI and T_a averaged across iButtons, during and after the heat wave. Differences between resultant slopes during and post-heat wave within each region were determined using analysis of covariance (ANCOVA). Wind speed data obtained from CIMIS stations were compared between day and night using *t*-tests. All analyses were conducted using Matlab (ver 7.12.0.635, MathWorks).

3. Results

At the microscale in 4-month averages, land covers with vegetation were cooler (smaller T_a) than a bare soil site and increasing vegetation resulted in increasing cooling effects (Fig. 2). The cooling effect was greatest for the tall tree plots relative to bare plots at 0.1 m height with a mean cooling of 4.0 ± 2.8 °C. A maximum difference of mean cooling between bare soil and tall tree plots of 6.9 °C occurred near the land surface at midday and a minimum difference of mean cooling of 2.0 °C occurred in the late afternoon (i.e., 1800 h). While the tall tree plots were always cooler than the bare plots at both measured heights (Fig. 2), differences between bare soil and both short tree and grass plots were not as consistently observed. At 0.1 m height grass and short trees were cooler than bare soil during the midday (4.6 and 6.7 °C mean differences respectively) and late afternoon periods (3.0 and 4.1 °C mean differences respectively), but not during night or early morning periods, suggesting the effectiveness of shading by the canopy. At the 2.0 m height samples, differences between the bare soil and grass or short tree plots were only observed at the midday period (2.2 and 2.3 °C mean differences, respectively), suggesting the effectiveness of boundary layer mixing. Additionally, the ground temperature was cooler underneath the tall trees (17.6 ± 3.6 °C) relative to the short trees (18.8 ± 3.3 °C) and reached a lower daytime maximum (26.8 ± 5.7 vs 27.9 ± 5.8 °C, respectively, Fig. 2). The local land cover differences in temperature were greatest closer to the land surface and underneath increasing vegetation cover.
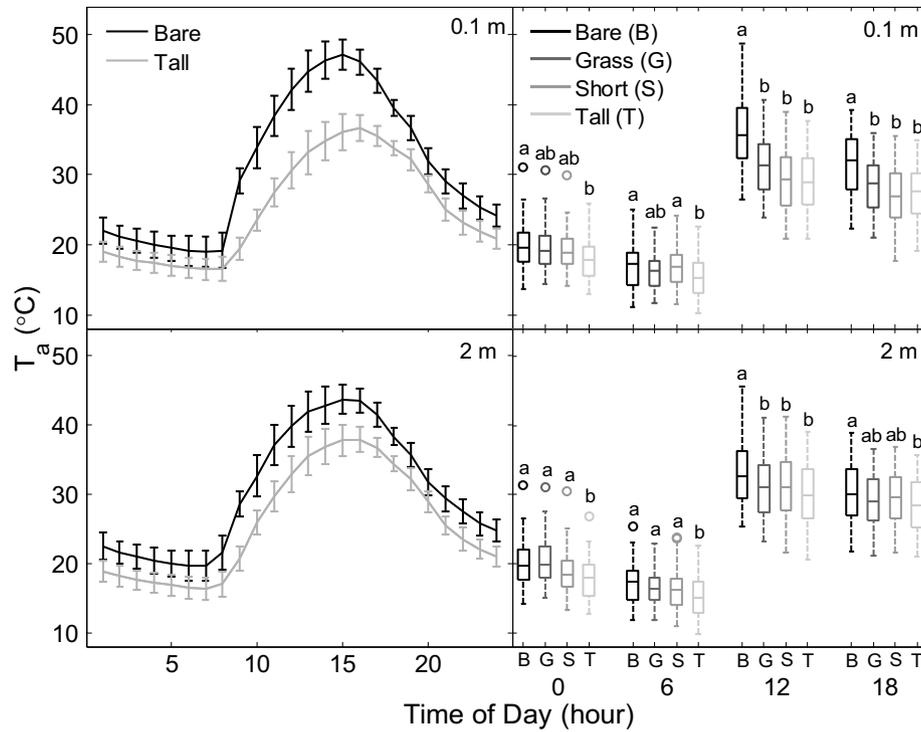
Fig. 2. Diel T_a at multiple heights (0.1 m and 2 m) above four land use types (B = bare ground, G = grass cover, S = short trees where canopy height ~2 m, and T = tall trees where canopy height ~4 m). Five-day averages of diel T_a above bare soil and tall tree plots at 0.1 m (top left) and 2 m (bottom left). T_a averages across the entire sampling period are shown at six hour intervals throughout the day above four land cover types at 0.1 m (top right) and 2 m (bottom right) heights.

Across the region, we observed consistent negative relationships between LST and NDVI (Fig. 3). However, significant differences among slopes were not observed ($F = 1.75$, $p = 0.18$). Mean LST, standardized by time of acquisition, increased across the coastal- to desert-gradient from 43.8 ± 3.1, to 46.8 ± 3.4, to 57.7 ± 4.2 °C in Los Angeles, Riverside, and Palm Springs, respectively (Figs. 3, 4). Mean and maximum NDVI, however, were fairly similar across the randomly sampled locations in each region, with the highest observed mean NDVI in Riverside at 0.30 ± 0.10, and the lowest in Palm Springs at 0.22 ± 0.11 (Fig. 3). Relationships between LST and T_a at 1300 h, a time when aerial remote sensing encompassed all sensors, had weak predictive power in Los Angeles and Riverside (i.e., $r^2 < 0.10$) and no relationship was observed between LST and T_a in Palm Springs. Thus, despite a wide range in LST in each region, ranges in T_a were relatively narrow. For example, LST varied in Los Angeles and Riverside, by as much as 13.4 and 16.6 °C, respectively, but T_a only varied by ~4 °C in each region during this timeframe; this contrast again suggests the importance of atmospheric mixing and dispersion of heat. In Palm Desert, a wider range was observed in both LST and T_a, where LST varied spatially as much as 21.2 °C, and T_a varied by 7.3 °C.

While nighttime T_a was similar between the Los Angeles and Riverside regions, during the day Riverside experienced higher maximum temperatures (Fig. 4). Excluding a late season heat wave, the highest daytime hourly average temperature in Riverside was 40.5 °C compared to 32.6 °C in Los Angeles. The Palm Springs region experienced both higher daytime maximum (44.8 °C, excluding a late season heat wave) and nighttime minimum temperatures (20.2 °C) than either Los Angeles (15.2 °C) or Riverside (14.5 °C). There was also more variation in T_a in Palm Springs, than either Los Angeles, or Riverside, as shown by a higher standard deviation throughout the day in Palm Springs relative to the other two regions (Fig. 4). Variability in T_a was more pronounced during night-to-day, and day-to-evening transitions in Los Angeles and Riverside, but in Palm Springs, higher variability occurred throughout the day more often than in the other two regions.

Across all three regions, T_a was related with both LST and NDVI, although the magnitude of the relationships varied within and between days (Fig. 5). T_a and LST were most consistently related in Los Angeles, and Riverside, but substantially less so in Palm Springs (70%, 71%, and 8% of all sampling periods, respectively). T_a and NDVI were most consistently related in Los Angeles and slightly less so in Riverside and Palm Springs (63%, 56%, and 56% of all sampling periods, respectively). In Los Angeles and Riverside, the fewest significant diel regressions between NDVI and T_a were observed between 0900 and 1600 h, whereas in Palm Springs, the distribution for significant versus non-significant relationships was more evenly distributed throughout the day. From 1000 to 1300 h, significant relationships between NDVI and T_a were observed on 60 days or more in Palm Springs, compared to fewer than 10 days in the other two regions.

Several heat waves are evident that span the entire region. A strong late season heat wave occurred on days 257–259 in September. During this period, maximum hourly temperature averaged across sampling locations exceeded 37.4 ± 1.4 °C in Los Angeles, 41.4 ± 0.8 °C in Riverside, and 42.6 ± 1.7 °C in Palm Springs. Unlike Los Angeles and Riverside, where the highest daytime maximum occurred during the late season heat wave, the highest daytime maximum air temperature occurred in Palm Springs during a July heat wave (DOY = 205).

Lapse rates, which compare the change in temperature relative to the change in height, of microscale plot data demonstrate differences among land cover types during the heat wave compared to after the heat wave (Fig. 6). Two-way ANOVAs comparing lapse rates at the various sites (i.e., bare, grass, short trees, or tall trees) and temperature regimes (i.e., heat wave, all data, and post-heat wave) revealed significant interactions between site and temperature regime both at night ($F = 5.884$, $p = 0.001$) and during the day ($F = 2.284$, $p = 0.035$). Post-hoc testing demonstrated that during both night and day, lapse rates were significantly different during a heat wave compared to all data or post-heat wave, where the latter two categories were not different from one another during the day. Furthermore, at night, the bare surface
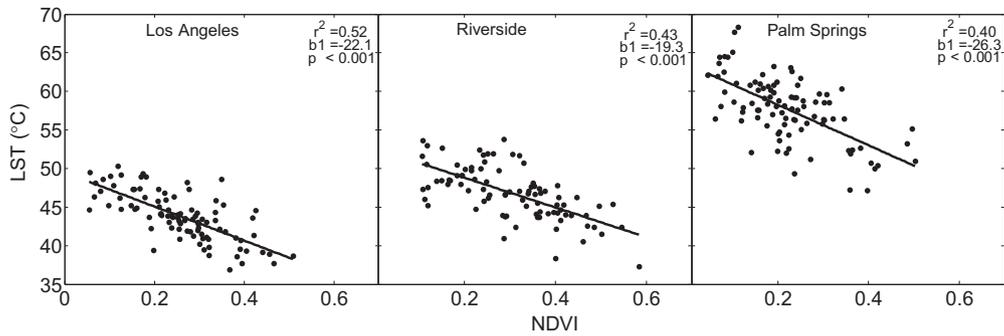
Fig. 3. Relationships between LST (°C) and NDVI in Los Angeles, Riverside, and Palm Springs. LST obtained at 1300 h, when flight lines captured all sites at approximately the same TOD, while NDVI was obtained from AVIRIS hyperspectral data captured from multiple flight lines.

and tall tree covered surfaces had similar lapse rates, whereas the short tree- and grass-covered surfaces were different from each other, as well as, from the other two surfaces. During the day, lapse rates of all vegetated surface groups were different from the bare soil group. The tall tree- and short tree-covered surfaces were also different from the grass-covered surfaces. For both the short and tall tree plots, lapse rates changed minimally at nighttime and changes were greater during the day. During the day, T_a at 0.1 m was warmer than at 2 m for both the bare and the grass plots, as evidenced by a negative lapse rate, but the opposite occurs for both types of tree plots, where the T_a at 0.1 m is cooler than at 2 m (Fig. 6). During heat waves, the skies were cloud-free and therefore, strong radiative cooling at night can lead to temperature inversion near the surface (especially over bare soil), which yields positive lapse rate at night. In contrast, during post heat-wave cloudy skies, clouds can absorb thermal radiation and emit it back to the surface, thereby rendering negative lapse rate at night.

Slope analysis comparing NDVI and T_a during the heat wave and on several days following the heat wave revealed that vegetation had a stronger effect (i.e., more negative slope) on T_a during periods of extreme warmth than during a cooler period (Fig. 7). This suggests that vegetation has an important role in coping with the effect of heat waves. No differences were observed during the middle of the day or evening (~0900–~1900 h), but nighttime differences were observed at 2300 h across cities (Fig. 7). In Los Angeles, slopes between NDVI and

T_a during the heat wave were different than those during the cool period primarily during the early morning (e.g., 0400–0800 h), and late at night (2300–2400 h), whereas in Riverside, differences in slopes were observed at night (e.g., from 2000 to 2400), and in the early morning (e.g., 0500 h). In Palm Desert, differences in pre- and post-heat wave slopes were confined to 1 h of the day (2300 h). However, differences between the late season heat wave and post-heat wave T_a at the hottest time of the day (i.e., 1500 h) were greater in Los Angeles (10 °C) and Riverside (12 °C), than in Palm Desert (5 °C).

4. Discussion

We found a substantial influence of vegetation on both LST and T_a across the dramatic climate gradient in southern California. At a microscale in the moderately arid inland region, increased vegetation cover reduced T_a, regardless of time of day and the effect was strongest closest to the land surface and during heat waves. These results were consistent with our predictions that increasing vegetation would decrease near surface temperatures and effects would be reduced with increasing height above the ground surface. However, in contrast to predictions of stronger land cover – LST coupling in hotter, more arid locations (Tayyebi and Jenerette, 2016), slope analysis showed that land cover – LST relationships were similar from the coast to the desert. Consistent with our predictions, we detected less coupling between LST and T_a
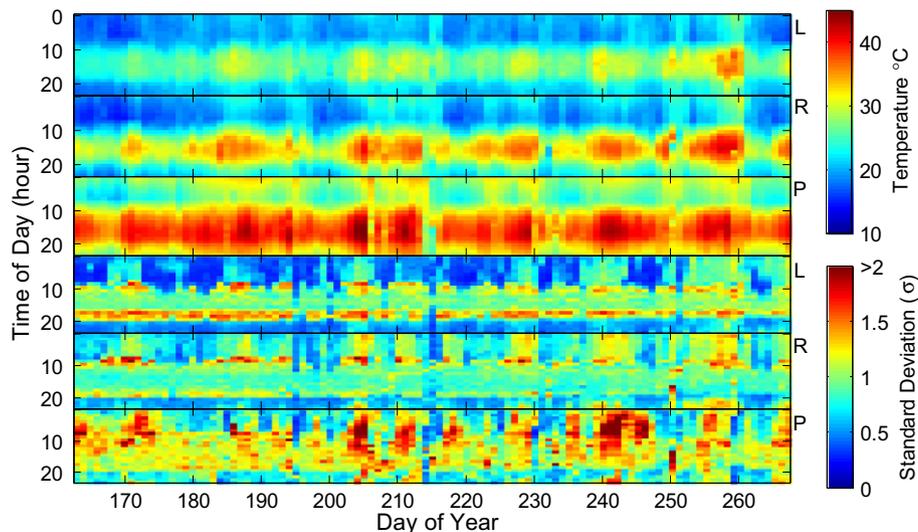

Fig. 4. Heatmap depicting hourly T_a (top three panels) throughout the study period and standard deviation of T_a (bottom three panels). Each pixel represents the average of all sensors within a given city where L = Los Angeles (n = 95), R = Riverside (n = 89), and P = Palm Springs (n = 94). The upper limit of the scale for standard deviation includes values >2.
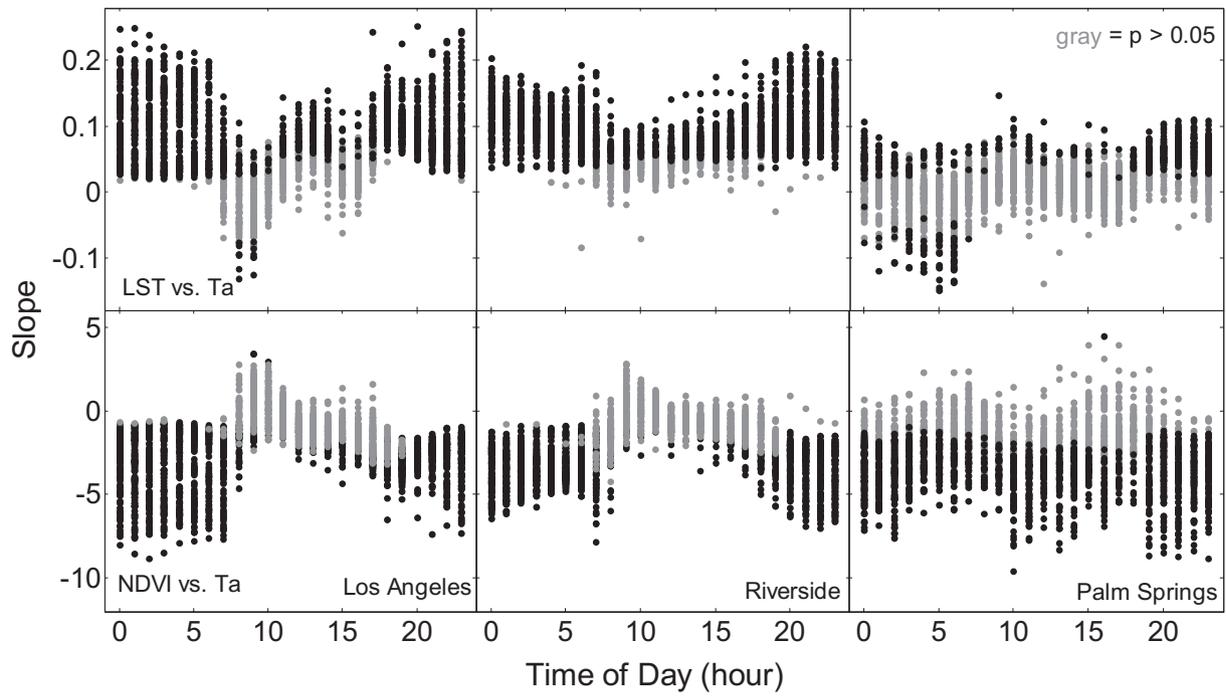
Fig. 5. Slope analysis between LST and T_a (top panels) and NDVI and T_a (bottom panels) for Los Angeles (right), Riverside (middle), and Palm Springs (right). Hourly, 105 regressions are displayed. Gray values represent regressions where $p > 0.05$.

across the climate gradient. Furthermore, while intra-urban LST is more closely connected with land cover during the day than at night (Myint et al., 2013; Jenerette et al., 2016) we found T_a is primarily influenced by land cover at night. Yet, in the desert, midday reductions in T_a associated with increasing vegetation cover occurred with greater frequency than in the other two regions. These finding show the time and space varying

Fig. 6. Lapse rate (i.e., $\Delta T_a/\Delta$ sensor height) over four land cover types during a late season heat wave, for all data, and in the period immediately following the heat wave during the night (i.e, from 2000 h–0700 h, top), and day (i.e., from 0800 h–1900 h, bottom).

relationships with the vegetation-LST-T_a nexus differentially respond to land cover and climate changes and may have distinct influences on human health and energy consumption patterns.

4.1. The vegetation-LST-T_a nexus

LST and T_a provide distinct indicators of climate that differ in magnitude of variation and response to meteorological and land cover patterns. Determination of surface temperature in cities is challenging due to the complex structure of the urban-atmosphere interface (Voogt and Oke, 2003). LST is measured using remote sensing techniques from a single time period and the height of the surface measurement can vary from a tree canopy or building roof to the ground. How the total active three dimensional urban surface characteristics influence LST measurements is unclear (Roth et al., 1989; Soux et al., 2004). At the same time, small-scale patterns in urban land cover patches and associated variability in thermal properties of each surface may contribute to a disconnect between LST and T_a, regardless of climate region. For example, each component surface in urban landscapes (e.g., lawn, parking lot, road, building, and vegetation canopy) exhibits unique radiative, thermal, moisture, and aerodynamic properties and contribute differentially to warming of air parcels (Oke, 1982). Previous work has shown that depending on the scale, spatiotemporal T_a patterns can be highly variable and complex due to the heterogeneity of environmental factors that control urban energy balance and microclimate systems (Oke, 1982; Benali et al., 2012).

The complexity in the relationships between urban warming indicators is in line with Voogt and Oke (2003), who found that while no simple general relation was observed between LST and T_a, correlations improved at night when microscale advection is reduced. In Palm Springs, relationships between LST and T_a were generally poor, yet, far more significant relationships were observed at night between 2000 and 2400 h. Other studies, which have sought to find relationships between LST and T_a, note the importance of micro-advection in the near-surface air layer, which promotes mixing of the thermal properties across a wider environment (Roth et al., 1989; Imhoff et al., 2010; Zhao et al., 2014). Air parcels warm at different rates and contribute
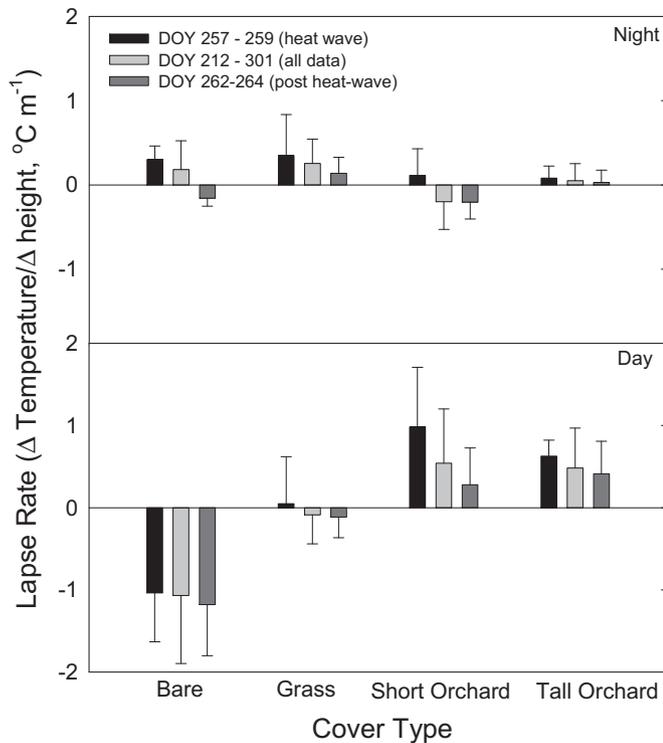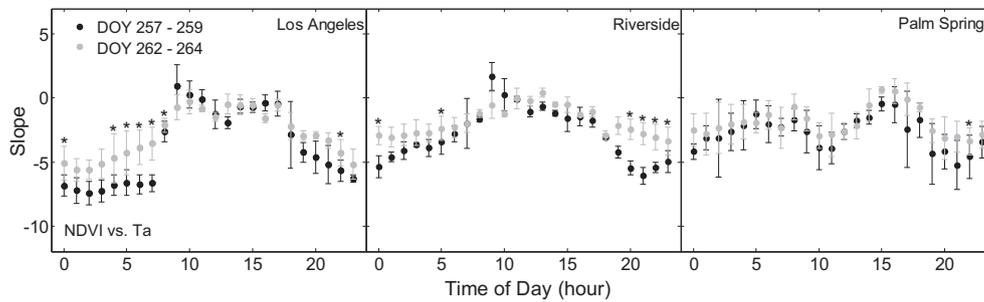
Fig. 7. Diel slope analysis comparing NDVI and T_a during a late season heat wave (DOY 257–259) and in the period immediately prior to the heat wave (DOY 262–264) for Los Angeles, Riverside, and Palm Springs. Slopes are displayed ±SD and * signifies $p < 0.05$.

differentially to mixing during the day, factors which make it challenging to establish a straightforward relationship between LST and T_a. Increases in vegetative cover lead to both increased ground shading and evaporative cooling, thus reducing LST and T_a by reducing the amount of land surface area exposed to absorb solar radiation and corresponding sensible heat flux.

Albedo is also an important parameter pertaining to the thermal aspects of vegetation and built environments because higher albedo of vegetated versus traditional built surfaces reduces solar heat load (Dimoudi and Nikolopoulou, 2003; Imhoff et al., 2010). By reducing the net incoming radiation, increased albedo provides cooling by lowering air and surface temperatures. Local and downwind ambient air temperatures are also reduced because of smaller convective heat fluxes from cooler surfaces (Taha, 1997). While albedo for vegetation generally varies between 0.09 and 0.25, species found in hot-dry climates with low rainfall and high evaporative demand have higher albedos than those in mesic environments (Dimoudi and Nikolopoulou, 2003). Deciduous species also tend to have higher albedo (e.g., 0.15 to 0.18) relative to coniferous species (i.e., 0.09 to 0.15) and grasses tend to have higher albedo (e.g., 0.20 to 0.25) relative to trees (Kessler and Jaeger, 1999; Coakley, 2002; Dimoudi and Nikolopoulou, 2003). The albedo of built surfaces varies greatly within an urban region, especially with adoption of green-roof and cool-roof heat mitigation strategies (Berardi, 2014; Georgescu et al., 2014). While albedo was not measured in our study, we expect it does contribute to the variability and degree of coupling between LST and T_a within and among urban regions. Future work is needed which not only quantifies species-specific cooling effects, but also accounts for the albedo of heterogeneous components of the built urban environment.

The built urban environment also influences radiant temperatures as the sky view factor (SVF), which expresses the ratio between radiation received by a planar surface and that from the entire hemispheric radiation environment, decreases with increasing obstructions (e.g., height and density of buildings) thereby slowing surface cooling during calm, cool nights (Oke, 1981; Svensson, 2004). We observed stronger relationships between LST and T_a when comparing daytime LST with nighttime T_a, as opposed to daytime T_a. Surfaces with higher daytime LST absorb and store more heat during the day and re-release more heat at night in the form of longwave radiation and convectively as sensible heat warming the surrounding air (Roth et al., 1989). Moreover, air is typically calmer at night, albeit less so in deserts, and air parcels are more likely to remain spatially closer to the surface where thermal transfer from the land surface occurs (Stull, 1988). Wind speed data, which show reduced nighttime wind velocities in Los Angeles and Riverside provide further support for the finding of higher degree of coupling between nighttime LST and T_a compared to daytime LST and T_a (Fig. 8). Similar day versus night wind speed in Palm Springs may also partially explain why fewer significant relationships between LST and T_a were observed daily relative to the other regions. Nevertheless, since global mean surface temperature, a fundamental measure of global warming, requires the use of measured T_a over land, the work here is

an important step toward understanding LST – T_a relationships in order to use satellite-based LST for globally mapping T_a.

At diel scales, relationships between maximum LST and T_a are more complex during the day than at night due to the dynamic inputs of solar radiation (Vogt et al., 1997; Czajkowski et al., 2000). Nocturnal intra-urban variability in LST is smaller than diel variability, while the opposite pattern occurs for variability of urban T_a (Unger et al., 2009). Thus, there appears to be a contradiction in how near-surface climates are connected to active surfaces in urban landscapes. Roth et al. (1989) posit this could be due to multiple reasons including the lack of a simple connection between LST and T_a values, remote sensors failing to capture the full active surface in urban areas, and failure to recognize the different scales of climatic phenomena. Accordingly, the complex relationships between LST and T_a were not unexpected.

Vegetation can have a strong influence on LST – T_a dynamics owing to the transfer of water and energy between land surface and atmosphere, partitioning incoming radiant energy into latent and sensible heat (Stisen et al., 2007; Mildrexer et al., 2011). At a microscale in the moderately arid inland region, increasing vegetation cover reduced T_a. Yet, reductions in temperature between bare soil and both grass and short tree plots were not consistently observed. Bare soil has higher temperatures in the day compared to vegetated surfaces due to a lack of shading and thus more absorption of radiant heat. At night, bare and vegetated surfaces reach equilibrium with T_a and approach similar temperatures as sensible heat is given off to the atmosphere. Additionally, the tall tree plots had a closed canopy, maximizing ground shading and minimizing solar irradiance reaching the ground surface, whereas the short tree plots consisted of individual trees, spaced ~1.5 m apart and lacking a closed canopy, enabling sunflecks to penetrate the canopy, thereby transferring more energy to the ground surface. Plant functional
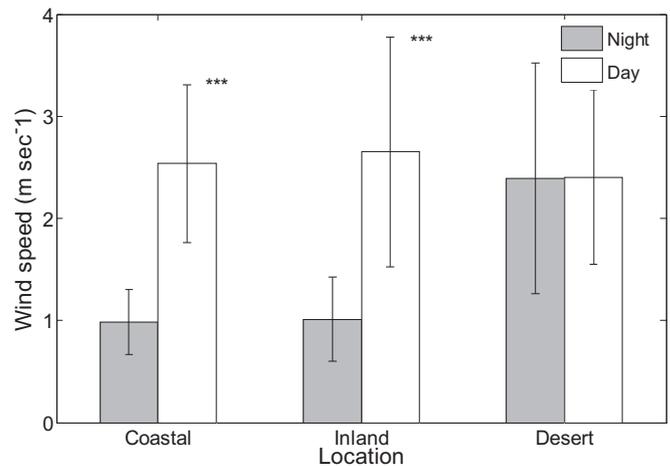

Fig. 8. Wind speed (m·sec⁻¹) during the night compared to the day at a coastal site, inland and in the desert. Weather stations were selected within 20 km of iButton sensors and were representative of the three sampled urban regions; *** signifies $p < 0.001$.

types also affect microclimate differently, leading to variation in diel cooling patterns (Armson et al., 2012). Differences in latent and sensible heat fluxes and albedos associated with bare, grass, and tree-covered surfaces translate into variation in LST and T_a associated with each land use type.

Our results at the regional scale contrast with other studies which demonstrate mid-afternoon reductions in T_a by vegetation (Souch and Souch, 1993; Hart and Sailor, 2009; Gillner et al., 2015), and studies which demonstrate that tree canopies can retain heat at night (Huang et al., 2008; Gillner et al., 2015). However, our results are consistent with findings showing vegetation primarily influences nighttime air cooling with limited effects during the day (Coseo and Larsen, 2014), especially in less arid regions. Higher evapotranspiration rates driven by a higher vapor pressure deficit in the more arid Palm Springs region may explain why slightly more than half of the days sampled showed mid-afternoon reductions in T_a with increasing vegetation compared to fewer than 10% in the other regions.

Vegetation is also one of many factors that affects lapse rate between LST and T_a (Jin and Dickinson, 2010; Benali et al., 2012). The interaction among factors such as vegetation, solar irradiance, soil moisture, soil emissivity, cloud fraction, and wind velocity contributes to weak relationships observed between LST and T_a (Huband and Monteith, 1986; Jin and Dickinson, 2010). Anthropogenic heat emissions such as from air conditioning units and automobiles introduce further complexity and variability into relationships between LST and T_a (Ohashi et al., 2007; Sailor, 2010). Lapse rates between LST and T_a likely vary regionally due to a range of combinations in their drivers, thereby altering the degree of coupling between LST and T_a. Understanding the differences in drivers of variability between LST and T_a and vegetated cooling effects among and within cities remains an ongoing challenge.

4.2. Scale dependence of urban vegetation – climate relationships

Increased vegetation cover reduces T_a at the microscale regardless of TOD, but the effects of vegetation on T_a at a regional scale demonstrate vegetated reductions in T_a limited to evening and nighttime hours in Los Angeles and Riverside, and throughout the day in Palm Springs. The patterns which emerge depend on the scale of study (Hewitt et al., 2010) and determination of the key scale(s) in which environmental processes operate is important for urban land cover – microclimate relationships (Jenerette et al., 2016). Not only does understanding gained by linking processes across scales influence our ability to predict change, but patterns that emerge at one scale can collapse to noise when observed at other scales (Hewitt et al., 2010). Such cross-scale differences were observed in our study, where strong linkages between increased vegetation cover and daytime T_a at the microscale were muted at the regional scale. Determining the factors which contribute to this breakdown will help us understand how information is transferred from a fine scale to a broad scale (Krönert et al., 2001). The importance of determining scale and examining cross-scale patterns is especially relevant in the context of regional effects of urbanization, increased warming and aridity, and associated relationships with energy balance phenomena.

4.3. Heat waves

The late season heat wave from DOY 257–259 set several records throughout the region and was associated with the highest electricity demand recorded in Los Angeles County. Utility officials reported demand on September 16, 2016 was at 6235 MW, which topped a record set the day before, and then previously on September 27, 2010 when demand was 6177 MW. The energy demand was nearly double the amount of energy experienced on a typical day in Los Angeles. Moreover, on September 15, 2014 downtown Los Angeles broke a nearly-century-old T_a record for the date with a high of 39.4 °C. Heat alerts, advisories, and warnings were released by many local agencies and cooling stations were opened throughout the region to help provide relief.

During heat wave events the role of potential climate mitigation strategies may be especially important for reducing temperatures and their negative consequences. Importantly, we found during the late-season heat wave the effectiveness of vegetation is consistently stronger in Los Angeles relative to the other two regions. This in part may be because temperature difference between the heat wave and post-heatwave was several degrees larger in Los Angeles and Riverside, relative to Palm Springs. These results demonstrate that as heat intensity increases within a region, vegetation effectiveness for cooling T_a also increases and acts as a potential negative climate feedback consistent with vegetation – LST relationships (Jenerette et al., 2013; Tayyebi and Jenerette, 2016). This vegetation-based negative climate feedback is in contrast to positive reinforcing effects of urban heat islands on heatwave meteorology (Li and Bou-Zeid, 2013). More research is needed to identify thresholds for heat-related cooling effectiveness, associated demands for water use, and variability in effectiveness among species.

4.4. Planning for cooler cities

Our data suggest initiatives to increase green cover in urban areas can mitigate urban warming and potentially reduce negative health and energy consumption consequences of high urban temperatures. In our study, data across multiple spatial and temporal scales indicate increased vegetation cover reduces air and surface temperatures. For instance, our microscale data demonstrate that vegetation may substantially offset T_a during the day, especially immediately above the land surface, while our regional scale analysis suggests large magnitudes of vegetated air cooling at night and surface cooling during the day. Our data also show that vegetation cooling effectiveness was increased during periods of extreme heat. Therefore, in looking to climate adaptations and heat mitigation, vegetation may have a beneficial role as a negative local climate feedback as the effectiveness of vegetation for cooling increases in warmer conditions. Efforts to increase vegetation in high heat risk regions may have valuable impacts on heat vulnerability (Jenerette et al., 2013; Vargo et al., in press).

Nevertheless, important constraints on cooling effectiveness need further investigation. For many regions, the water requirements of vegetation can be large and represent an important trade-off for cooling through vegetation (Gober et al., 2010; Jenerette et al., 2013). Vegetation can differ dramatically in provisioning of cooling; as we showed here grass and trees provide contrasting cooling effects. Previous work supports the importance of plant functional type differences in cooling (Jenerette et al., 2016) and many trait differences within plants of the same type could also influence production of cooling services and associated water use trade-offs (McCarthy et al., 2011). Further, the arrangement of vegetation may also influence optimal cooling benefits (Zhou et al., 2011; Li et al., 2016). Clustering vegetation closer together may provide enhanced cooling benefits relative to vegetation that is distributed father apart because vegetation that forms a closed canopy will increase albedo and reduce the amount of radiative energy absorbed and re-emitted by the land surface. The taller tree plots in this study, which were also linked with the highest cooling effectiveness, had a closed canopy, while the other vegetation cover classes did not. Initiatives to increase urban green coverage should therefore consider plant functional characteristics and arrangement to maximize urban cooling benefits.

4.5. Conclusion

While vegetation can be an effective approach for reducing both T_a and LST, the complexities in urban climate variation are large. Identifying relationships between LST and T_a has been an important research need within urban and global climate studies where satellite-based

LST data are readily available. Here we show T_a and LST are complementary and linked climate indicators that differ in magnitudes of variation and correlations with land cover characteristics. Vegetation had variable cooling effects on both LST and T_a that depended on both spatial and temporal contexts. Working across a dramatic climate gradient spanning mild coastal to extreme desert conditions allowed our study to serve as a valuable case study directly relevant to the 18 million residents in the region and as a model system for other cities in diverse climate conditions. In looking to retrofit current urban environments and build new urban infrastructure for the projected large increases in urban residents, reducing potential heat impacts from combined global and regional warming is a crucial sustainability challenge.

Acknowledgements

References

Armson, D., Stringer, P., Ennos, A.R., 2012. The effect of tree shade and grass on surface and globe temperatures in an urban area. Urban For. Urban Green. 11:245–255. http://dx.doi.org/10.1016/j.ufug.2012.05.002.

Benali, A., Carvalho, A.C., Nunes, J.P., Carvalhais, N., Santos, A., 2012. Estimating air surface temperature in Portugal using MODIS LST data. Remote Sens. Environ. 124:108–121. http://dx.doi.org/10.1016/j.rse.2012.04.024.

Berardi, U., 2014. State-of-the-art analysis of the environmental benefits of green roofs. Appl. Energy 115:411–428. http://dx.doi.org/10.1016/j.apenergy.2013.10.047.

Buyantuyev, A., Wu, J.G., 2010. Urban heat island and landscape heterogeneity: linking spatiotemporal variations in surface temperature to land-cover and socioeconomic patterns. Landsc. Ecol. 25:17–33. http://dx.doi.org/10.1007/s10980-009-9402-4.

Cheng, K.S., Su, Y.F., Kuo, F.T., Hung, W.C., Chiang, J.L., 2008. Assessing the effect of landcover changes on air temperature using remote sensing images – a pilot study in northern Taiwan. Landsc. Urban Plan. 86, 85–96.

Clarke, L.W., Jenerette, G.D., Davila, A., 2013. The luxury of vegetation and the legacy of tree biodiversity in Los Angeles, CA. Landsc. Urban Plan. 116, 48–59.

Coakley, J.A., 2002. In: Holton, J.R., Curry, J.A., Pyle, J.A. (Eds.), Reflectance and albedo. Encyclopedia of the atmospheric sciences. Academic Press, pp. 1914–1923.

Coseo, P., Larsen, L., 2014. How factors of land use/land cover, building configuration, and adjacent heat sources and sinks explain Urban Heat Islands in Chicago. Landsc. Urban Plan. 125:117–129. http://dx.doi.org/10.1016/j.landurbplan.2014.02.019.

Czajkowski, K.P., Goward, S.N., Stadler, S.J., Walz, A., 2000. Thermal remote sensing of near surface environmental variables: application over the Oklahoma Mesonet. Prof. Geogr. 52:345–357. http://dx.doi.org/10.1111/0033-0124.00230.

Declet-Barreto, J., Knowton, K., Jenerette, G.D., Buyantuyev, A., 2016. Effects of urban vegetation on mitigating exposure of vulnerable populations to excessive heat in Cleveland, Ohio. Weather Clim. Soc. (online first) (doi:10.1175.WCAS-D-15-0026.1).

Dimoudi, A., Nikolopoulou, M., 2003. Vegetation in the urban environment: microclimatic analysis and benefits. Energy Build. 35:69–76. http://dx.doi.org/10.1016/S0378-7788(02)00081-6.

Doick, K.J., Peace, A., Hutchings, T.R., 2014. The role of one large greenspace in mitigating London's nocturnal urban heat island. Sci. Total Environ. 492:662–671. http://dx.doi.org/10.1016/j.scitotenv.2014.06.048.

Feyisa, G.L., Dons, K., Meilby, H., 2014. Efficiency of parks in mitigating urban heat island effect: an example from Addis Ababa. Landsc. Urban Plan. 123:87–95. http://dx.doi.org/10.1016/j.landurbplan.2013.12.088.

Georgescu, M., Morefield, P.E., Bierwagen, B.G., Weaver, C.P., 2014. Urban adaptation can roll back warming of emerging megapolitan regions. Proc. Natl. Acad. Sci. U. S. A. 111: 2909–2914. http://dx.doi.org/10.1073/pnas.1322280111.

Gillner, S., Vogt, J., Tharang, A., Dettman, S., Roloff, A., 2015. Role of street trees in mitigating effects of heat and drought at highly sealed urban sites. Landsc. Urban Plan. 143: 33–42. http://dx.doi.org/10.1016/j.landurbplan.2015.06.005.

Gober, P., Brazel, A., Quay, R., Myint, S., Grossman-Clarke, S., Miller, A., Rossi, S., 2010. Using watered landscapes to manipulate urban heat island effects: how much water will it take to cool Phoenix? J. Am. Plan. Assoc. 76, 109–121.

Grundström, M., Pleijel, H., 2014. Limited effect of urban tree vegetation on NO$_2$ and O$_3$ concentrations near a traffic route. Environ. Pollut. 189:73–76. http://dx.doi.org/10.1016/j.envpol.2014.02.026.

Hall, S.J., Learned, J., Ruddell, B., Larson, K.L., Cavender-Bares, J., Bettez, N., Groffman, P.M., Grove, J.M., Heffernan, J.B., Hobbie, S.E., Morse, J.L., Neill, C., Nelson, K.C., O'Neil-Dunne, J.P.M., Ogden, L., Pataki, D.E., Pearse, W.D., Polsky, C., Chowdhury, R.R., Steele, M.K., Trammell, T.L.E., 2016. Convergence of microclimate in residential landscapes across diverse cities in the United States. Landsc. Ecol. 31:101–117. http://dx.doi.org/10.1007/s10980-015-0297-y.

Harlan, S.L., Chowell, G., Yang, S., Petitti, D.B., Morales Butler, E.J., Ruddell, B.L., Ruddell, D.M., 2014. Heat-related deaths in hot cities: estimates of human tolerance to high temperature thresholds. Int. J. Environ. Res. 11:3304–3326. http://dx.doi.org/10.3390/ijerph110303304.

Hart, M.A., Sailor, D.J., 2009. Quantifying the influence of land-use and surface characteristics on spatial variability in the urban heat island. Theor. Appl. Climatol. 95: 397–406. http://dx.doi.org/10.1007/s00704-008-0017-5.

Hartz, D.A., Prashad, L., Hedquist, B.C., Golden, J., Brazel, A.J., 2006. Linking satellite images and hand-held infrared thermography to observed neighborhood climate conditions. Remote Sens. Environ. 104:190–200. http://dx.doi.org/10.1016/j.rse.2005.12.019.

Hewitt, J.E., Thrush, S.F., Lundquist, C., 2010. Scale-dependence in ecological systems. Encyclopedia of Life Sciences. Chichester, John Wiley & Sons, Ltd http://dx.doi.org/10.1002/9780470015902.a0021903.

Hondula, D.M., Barnett, A.G., 2014. Heat-related morbidity in Brisbane, Australia: spatial variation and area-level predictors. Environ. Health Perspect. 122:831–836. http://dx.doi.org/10.1289/ehp.1307496.

Hook, S.J., Myers, J.E.J., Thome, K.J., Fitzgerald, M., Kahle, A.B., 2001. The MODIS/ASTER airborne simulator (MASTER)—a new instrument for earth science studies. Remote Sens. Environ. 76:93–102. http://dx.doi.org/10.1016/S0034-4257(00)00195-4.

Huang, L., Li, J., Zhao, D., Zhu, J., 2008. A fieldwork study on the diurnal changes of urban microclimate in four types of ground cover and urban heat island of Nanjing, China. Buld. Environ. 43:7–17. http://dx.doi.org/10.1016/j.buildenv.2006.11.025.

Huang, G.L., Zhou, W.Q., Cadenasso, M.L., 2011. Is everyone hot in the city? Spatial pattern of land surface temperatures, land cover and neighborhood socioeconomic characteristics in Baltimore, MD. J. Environ. Manag. 92, 1753–1759.

Huband, N.D.S., Monteith, J.L., 1986. Radiative surface temperature and energy balance of a wheat canopy II: estimating fluxes of sensible and latent heat. Bound.-Layer Meteorol. 36:1–17. http://dx.doi.org/10.1007/BF00117462.

Huete, A., Didan, K., Miura, T., Rodriquez, E.P., Gao, X., Ferreira, L.G., 2002. Overview of the radiometric and biophysical performance of the MODIS vegetation indices. Remote Sens. Environ. 83:195–213. http://dx.doi.org/10.1016/S0034-4257(02)00096-2.

Imhoff, M.L., Zhang, P., Wolfe, R.E., Bounoua, L., 2010. Remote sensing of the urban heat island effect across biomes in the continental USA. Remote Sens. Environ. 114: 504–513. http://dx.doi.org/10.1016/j.rse.2009.10.008.

Jenerette, G.D., Potere, D., 2011. Global analysis and simulation of land-use change associated with urbanization. Landsc. Ecol. 25:657–670. http://dx.doi.org/10.1007/s10980-010-9457-2.

Jenerette, G.D., Harlan, S.L., Brazel, A., Jones, N., Larsen, L., Stefanov, W.L., 2007. Regional relationships between surface temperature, vegetation, and human settlement in a rapidly urbanizing ecosystem. Landsc. Ecol. 22:353–365. http://dx.doi.org/10.1007/s10980-006-9032-z.

Jenerette, G.D., Miller, G., Buyantuev, A., Pataki, D.E., Gillespie, T.W., Pincetl, S., 2013. Urban vegetation and income segregation in drylands: a synthesis of seven metropolitan regions in the southwestern United States. Environ. Res. Lett. 8:044001. http://dx.doi.org/10.1088/.1748-9326/8/4/044001.

Jenerette, G.D., Harlan, S.L., Buyantuev, A., Stefanov, W.L., Declet-Barreto, J., Ruddell, B.L., Myint, S., Kaplan, S., Li, X., 2016. Microscale urban surface temperatures are related to land cover features and heat related health impacts in Phoenix, AZ USA. Landsc. Ecol. 31:745–760. http://dx.doi.org/10.1007/s10980-015-0284-3.

Jin, M., Dickinson, R.E., 2010. Land surface skin temperature climatology: benefitting from the strengths of satellite observations. Environ. Res. Lett. 5:041002. http://dx.doi.org/10.1088/1748-9326/5/4/044004.

Johnson, A.N., Boer, B.R., Woessner, W.M., Stanford, J.A., Poole, G.C., Thomas, S.A., O'Daniel, S.J., 2005. Evaluation of an inexpensive small-diameter temperature logger for documenting ground water-river interactions. Ground Water Monit. Remediat. 25: 68–74. http://dx.doi.org/10.1111/j.1745-6592.2005.00049.x.

Kalkstein, L.S., 1991. A new approach to evaluate the impact of climate on human mortality. Environ. Health Perspect. 96:145–150. http://dx.doi.org/10.1289/ehp.9196145.

Kalnay, E., Cai, M., 2003. Impact of urbanization and land-use change on climate. Nature 423, 528–531.

Kawashima, S., Ishida, T., Minomura, M., Miwa, T., 2000. Relations between surface temperature and air temperature on a local scale during winter nights. J. Appl. Meteorol. 39:1570–1579. http://dx.doi.org/10.1175/1520-0450(2000)039<1570:RBSTAA>2.0.CO;2.

Kessler, A., Jaeger, L., 1999. Long-term changes in net radiation and its components above a pine forest and a grass surface in Germany. Int. J. Climatol. 19:211–226. http://dx.doi.org/10.1002/(SICI)1097-0088(199902)19:2<211::AID-JOC351>3.0.CO;2-1.

Klemm, W., Heusinkveld, B.G., Lenzholzer, S., van Hove, B., 2015. Street greenery and its physical and psychological impact on thermal comfort. Landsc. Urban Plan. 138: 87–98. http://dx.doi.org/10.1016/j.landurbplan.2015.02.009.

Krönert, R., Steinhardt, U., Volk, M., 2001. Landscape Balance and Landscape Assessment. Springer, New York http://dx.doi.org/10.1007/978-3-662-04532-9.

Kurn, D.M., Bretz, S.E., Huang, B., Akbari, H., 1994. The potential for reducing urban air temperatures and energy consumption through vegetative cooling. Lawrence Berkeley National Laboratory Report LBL-35320. CA, Berkeley http://dx.doi.org/10.2172/10180633.

Laaidi, K., Zeghnoun, A., Dousset, B., Bretin, P., Vandentorren, S., Giraudet, E., Beaudeau, P., 2012. The impact of heat islands on mortality in Paris during the August 2003 heatwave. Environ. Health Perspect. 120:245–259. http://dx.doi.org/10.1289/ehp.1103532.

Larsen, L., 2015. Urban climate and adaptation strategies. Front. Ecol. Environ. 13: 486–492. http://dx.doi.org/10.1890/150103.

Lee, C.M., Cable, M., Hook, S.J., Middleton, E.M., 2015. An introduction to the NASA Hyperspectral InfraRed Imager (HyspIRI) mission and preparatory activities. Remote Sens. Environ. 167:6–19. http://dx.doi.org/10.1016/j.rse.2015.06.01.

Li, D., Bou-Zeid, E., 2013. Synergistic interactions between urban heat islands and heat waves; the impact in cities is larger than the sum of the parts. J. Appl. Meteorol. Climatol. 52:2051–2064. http://dx.doi.org/10.1175/JAMC-D-13-02.1.

Li, X.X., Li, W.W., Middel, A., Harlan, S.L., Brazel, A.J., Turner, B.L., 2016. Remote sensing of the surface urban heat island and land architecture in Phoenix, Arizona: combined effects of land composition and configuration and cadastral-demographic-economic factors. Remote Sens. Environ. 174:233–243. http://dx.doi.org/10.1016/j.rse.2015.12.022.

McCarthy, H.R., Pataki, D.E., Jenerette, G.D., 2011. Plant water-use efficiency as a metric of urban ecosystem services. Ecol. Appl. 21:3115–3127. http://dx.doi.org/10.1890/11-0048.1.

McPherson, E.G., Simpson, J.R., Xiao, Q., Wu, C., 2011. Million trees Los Angeles canopy cover and benefit assessment. Landsc. Urban Plan. 99:40–50. http://dx.doi.org/10.1016/j.landurbplan.2010.08.011.

Mildrexer, D.J., Zhao, M., Running, S.W., 2011. A global comparison between station air temperatures and MODIS land surface temperatures reveals the cooling role forests. J. Geophys. Res. 116, G03025. http://dx.doi.org/10.1029/2010JG001486.

Myint, S.W., Wentz, E.A., Brazel, A.J., Quattrochi, D.A., 2013. The impact of distinct anthropogenic and vegetation features on urban warming. Landsc. Ecol. 28:959–978. http://dx.doi.org/10.1007/s10980-013-9868-y.

Ohashi, Y., Genchi, Y., Kondo, H., Hirano, Y., 2007. Influence of air-conditioning waste heat on air temperature in Tokyo during summer: numerical experiments using an urban canopy model coupled with a building energy model. J. Appl. Meteorol. Climatol. 46: 66–81. http://dx.doi.org/10.1175/JAM2441.1.

Oke, T.R., 1973. City size and urban heat island. Atmos. Environ. 7:769–779. http://dx.doi.org/10.1016/0004-6981(73)90140-6.

Oke, T.R., 1981. Canyon geometry and the nocturnal urban heat island: comparison of scale model and field observations. J. Climatol. 1:237–254. http://dx.doi.org/10.1002/joc.3370010304.

Oke, T.R., 1982. The energetic basis of the urban heat island. Q. J. R. Meteorol. Soc. 108: 1–24. http://dx.doi.org/10.1002/qj.49710845502.

Petralli, M., Massetti, L., Brandani, G., Orlandini, S., 2014. Urban planning indicators: useful tools to measure the effect of urbanization and vegetation on summer air temperatures. Int. J. Climatol. 34:1236–1244. http://dx.doi.org/10.1002/joc.3760.

Roberts, D.A., Quattrochi, D.A., Hulley, G.C., Hook, S.J., Green, R.O., 2012. Synergies between VSWIR and TIR data for the urban environment: an evaluation of the potential for the Hyperspectral Infrared Imager (HyspIRI) Decadal Survey mission. Remote Sens. Environ. 117:83–101. http://dx.doi.org/10.1016/j.rse.2011.07.021.

Roberts, D.A., Dennison, P.E., Roth, K.L., Dudley, K., Hulley, G., 2015. Relationships between dominant plant species, fractional cover and land surface temperature in a Mediterranean ecosystem. Remote Sens. Environ. 167:152–167. http://dx.doi.org/10.1016/j.rse.2015.01.026.

Roth, M., Oke, T.R., Emery, W.J., 1989. Satellite-derived urban heat islands from three coastal cities and the utilization of such data in urban climatology. Int. J. Remote Sens. 10:1699–1720. http://dx.doi.org/10.1080/01431168908904002.

Sailor, D.J., 2010. A review of methods for estimating anthropogenic heat and moisture emissions in the urban environment. Int. J. Climatol. 31:189–199. http://dx.doi.org/10.1002/joc.2106.

Santamouris, M., 2014. Cooling the cities – a review of reflective and green roof mitigation technologies to fight heat island and improve comfort in urban environments. Sol. Energy 103:682–703. http://dx.doi.org/10.1016/j.solener.2012.07.003.

Santamouris, M., 2015. Analyzing the heat island magnitude and characteristics in one hundred Asian and Australian cities and regions. Sci. Total Environ. 512–513: 582–598. http://dx.doi.org/10.1016/j.scitotenv.2015.01.060.

Santamouris, M., Papanikolaou, N., Livada, I., Koronakis, I., Georgakis, C., Argiriou, A., Assimakopoulos, D.N., 2001. On the impact of urban climate on the energy consumption of buildings. Sol. Energy 70:201–216. http://dx.doi.org/10.1016/S0038-092X(00)00095-5.

Schwarz, N., Schlink, U., Franck, U., Großmann, K., 2012. Relationship of land surface and air temperatures and its implications for quantifying urban heat island indicators - an application for the city of Leipzig (Germany). Ecol. Indic. 18:693–704. http://dx.doi.org/10.1016/j.ecolind.2012.01.001.

Skelhorn, C., Lindley, S., Levermore, G., 2014. The impact of vegetation types on air and surface temperatures in a temperate city: a fine scale assessment in Manchester, UK. Landsc. Urban Plan. 121:129–140. http://dx.doi.org/10.1016/j.landurbplan.2013.09.012.

Souch, C.A., Souch, C., 1993. The effect of trees on summertime below canopy urban climates: a case study Bloomington, Indiana. J. Arboric. 19, 303–312.

Soux, A., Voogt, J.A., Oke, T.R., 2004. A model to calculate what a remote sensor 'sees' of an urban surface. Bound.-Layer Meteorol. 111:109–132. http://dx.doi.org/10.1023/B:BOUN.0000010995.62115.46.

Stabler, L.B., Martin, C.A., Brazel, A.J., 2005. Microclimates in a desert city were related to land use and vegetation index. Urban For. Urban Green. 3:137–147. http://dx.doi.org/10.1016/j.ufug.2004.11.001.

Stisen, S., Sanholt, I., Nørgaard, A., Fensholt, R., Eklundh, L., 2007. Estimation of diurnal air temperature using MSG SEVIRI data in West Africa. Remote Sens. Environ. 110: 262–274. http://dx.doi.org/10.1016/j.rse.2007.02.025.

Stull, R.B., 1988. An Introduction to Boundary Layer Meterology. Kluwer Academic Publishers, Springer Netherlands http://dx.doi.org/10.1007/978-94-009-3027-8.

Svensson, M.K., 2004. Sky view factor analysis – implications for urban air temperature differences. Meteorol. Appl. 11:201–211. http://dx.doi.org/10.1017/S1350482704001288.

Svensson, M.K., Eliasson, I., 2002. Diurnal air temperatures in built-up areas-an urban planning perspective. Landsc. Urban Plan. 61, 37–54.

Taha, H., 1997. Urban climates and heat islands: albedo, evapotranspiration, and anthropogenic heat. Energy Build. 25:99–103. http://dx.doi.org/10.1016/S0378-7788(96)00999-1.

Tayyebi, A., Jenerette, G.D., 2016. Increases in the climate change adaption effectiveness and availability of vegetation across a coastal to desert climate gradient in metropolitan Los Angeles, CA, USA. Sci. Total Environ. 548-549:60–71. http://dx.doi.org/10.1016/j.scitotenv.2016.01.049.

Tucker, C.J., 1979. Red and photographic infrared linear combinations for monitoring vegetation. Remote Sens. Environ. 8, 127–150.

Unger, J., Gal, T., Rakonczai, J., Mucsi, L., Szatmári, J., Tobak, Z., van Leeuwen, B., Fiala, K., 2009. Air temperature versus surface temperature in urban environment. The Seventh International Conference on Urban Climate. Yokohama, Japan.

Upmanis, H., Eliasson, I., Lindqvist, S., 1998. The influence of green areas on nocturnal tempearatures in a high latitude city (Göteborg, Sweden). Int. J. Climatol. 18: 681–700. http://dx.doi.org/10.1002/(SICI)1097-0088(199805)18:6<681::AID-JOC289>3.0.CO;2-L.

Vanos, J.K., 2015. Children's health and vulnerability in outdoor microclimates: a comprehensive review. Environ. Int. 76:1–15. http://dx.doi.org/10.1016/j.envint.2014.11.016.

Vanos, J.K., Middel, A., McKercher, G.R., Kuras, E.R., Ruddell, B.L., 2016. Hot playgrounds and children's health: a multiscale analysis of surface temperatures in Arizona, USA. Landsc. Urban Plan. 146, 29–42.

Vargo, J, Stone B, Habeeb D, Liu P, and A Russell. The social and spatial distribution of temperature-related health impacts from urban heat island reduction policies. Environ. Sci. Pol. 66, 366–374, http://dx.doi.org/10.1016/j.envsci.2016.08.012 (in press)

Vogt, J.V., Viau, A.A., Paquet, F., 1997. Mapping regional air temperature fields using satellite-derived surface skin temperatures. Int. J. Climatol. 17:1559–1579. http://dx.doi.org/10.1002/(SICI)1097-0088(19971130)17:14<1559::AID-JOC211>3.0.CO;2-5.

Voogt, J.A., Oke, T.R., 2003. Thermal remote sensing of urban climates. Remote Sens. Environ. 86, 370–384 (doi:10.1016.S0034-4257(03)00079-8).

Wang, Y.F., Bakker, F., de Groot, R., Wortche, H., Leemans, R., 2015. Effects of urban trees on local outdoor microclimate: synthesizing field measurements by numerical modelling. Urban Ecosyst. 18:1305–1331. http://dx.doi.org/10.1007/s11252-015-0447-7.

Weng, Q., Yang, S., 2004. Managing the adverse thermal effects of urban development in a densely populated Chinese city. J. Environ. Manag. 70:145–156. http://dx.doi.org/10.1016/j.jenvman.2003.11.006.

Xu, T., Sathaye, J., Akbari, H., Garg, V., Tetali, S., 2012. Quantifying the direct benefits of cool roofs in an urban setting: reduced cooling energy use and lowered greenhouse gas emissions. Build. Environ. 48:1–6. http://dx.doi.org/10.1016/j.buildenv.2011.08.011.

Yan, H., Fan, S.X., Guo, C.X., Hu, J., Dong, L., 2014. Quantifying the impact of land cover composition on intra-urban air temperature variations at a Mid-Latitude City. PLoS One 9, e102124. http://dx.doi.org/10.1371/journal.pone.0102124.

Zhao, L., Lee, X., Smith, R.B., Oleson, K., 2014. Strong contributions of local background climate to urban heat islands. Nature 511:216–219. http://dx.doi.org/10.1038/nature13462.

Zhou, W.Q., Huang, G.L., Cadenasso, M.L., 2011. Does spatial configuration matter? Understanding the effects of land cover pattern on land surface temperature in urban landscapes. Landsc. Urban Plan. 102, 54–63.